




Scanning tunneling microscopy in the field-emission regime: Formation of a two-dimensional electron cascade

Journal Article

Author(s):

Werner, Wolfgang S. M.; Oral, Martin; Radlička, Tomáš; Zelinka, Jiří; Müllerová, Ilona; [Bellissimo, Alessandra](#) ; [Bertolini, Gabriele](#) ; [Cabrera, Hugo](#); [Gürlü, Oguzhan](#) 

Publication date:

2019-12-16

Permanent link:

<https://doi.org/10.3929/ethz-b-000387255>

Rights / license:

[Creative Commons Attribution 4.0 International](#)

Originally published in:

Applied Physics Letters 115(25), <https://doi.org/10.1063/1.5128300>

Funding acknowledgement:

606988 - Sources, Interaction with Matter, Detection and Analysis of Low Energy Electrons 2 (EC)

Scanning tunneling microscopy in the field-emission regime: Formation of a two-dimensional electron cascade

Cite as: Appl. Phys. Lett. **115**, 251604 (2019); <https://doi.org/10.1063/1.5128300>

Submitted: 19 September 2019 . Accepted: 05 December 2019 . Published Online: 17 December 2019

Wolfgang S. M. Werner , Martin Oral , Tomáš Radlička , Jiří Zelinka, Ilona Müllerová , Alessandra Bellissimo , Gabriele Bertolini , Hugo Cabrera , and Oguzhan Gürlü 



View Online



Export Citation



CrossMark

ARTICLES YOU MAY BE INTERESTED IN

Strain engineering on the metal-insulator transition of VO_2/TiO_2 epitaxial films dependent on the strain state of vanadium dimers

Applied Physics Letters **115**, 251605 (2019); <https://doi.org/10.1063/1.5121876>

Low-voltage MEMS optical phase modulators and switches on an indium phosphide membrane on silicon

Applied Physics Letters **115**, 251104 (2019); <https://doi.org/10.1063/1.5128212>

Ultrasensitive detection of ion concentration based on photonic spin Hall effect

Applied Physics Letters **115**, 251102 (2019); <https://doi.org/10.1063/1.5130729>



Lock-in Amplifiers

Zurich Instruments

Watch the Video

Scanning tunneling microscopy in the field-emission regime: Formation of a two-dimensional electron cascade

Cite as: Appl. Phys. Lett. **115**, 251604 (2019); doi: [10.1063/1.5128300](https://doi.org/10.1063/1.5128300)

Submitted: 19 September 2019 · Accepted: 5 December 2019 ·

Published Online: 17 December 2019



View Online



Export Citation



CrossMark

Wolfgang S. M. Werner,^{1,a)}  Martin Oral,²  Tomáš Radlička,²  Jiří Zelinka,²  Ilona Müllerová,² 
Alessandra Bellissimo,³  Gabriele Bertolini,³  Hugo Cabrera,³  and Oguzhan Gürlü,⁴ 

AFFILIATIONS

¹Institut für Angewandte Physik, TU Vienna, Wiedner Hauptstraße 8-10/134, A1040 Vienna, Austria

²Institute of Scientific Instruments of the CAS, Královopolská 147, 612 00 Brno, Czech Republic

³Laboratorium für Festkörperphysik, ETH Zürich, Auguste-Piccard-Hof 1, 8093 Zürich, Switzerland

⁴Department of Physics, Istanbul Technical University, Maslak, 34469 Istanbul, Turkey

^{a)}Electronic mail: werner@iap.tuwien.ac.at, fax: +43-1-58801-13499.

ABSTRACT

The signal generation mechanism of the scanning field-emission microscope has been investigated via model calculations combining deterministic trajectory calculations in the field surrounding the field-emission tip in vacuum, with Monte Carlo simulations of the electron transport inside the solid. This model gives rise to a two-dimensional electron cascade. Individual trajectories of detected backscattered electrons consist of repeated segments of travel in vacuum followed by a re-entry into the solid and re-emission into vacuum after being elastically or inelastically scattered. These so-called electron bouncing events also create secondary electrons at macroscopic distances away from the primary impact position. The signal reaching the detector is made up of elastically and inelastically backscattered primary electrons created near the impact position under the tip and those secondary electrons created far away from it.

© 2019 Author(s). All article content, except where otherwise noted, is licensed under a Creative Commons Attribution (CC BY) license (<http://creativecommons.org/licenses/by/4.0/>). <https://doi.org/10.1063/1.5128300>

Over the past century, electron microscopy (EM) has played a paramount role in making the invisible visible. When secondary electrons are used for imaging, this technique is referred to as secondary electron microscopy and is associated with a three-dimensional cascade¹ in which electron scattering leads to the formation of the escaping signal electrons by transferring energy and momentum to the solid state electrons. Conventional EM-techniques derive their resolving power in the sub-Ångström range from electron optics dealing with high acceleration voltages of typically a few hundred thousand volts.² In recent decades, lensless electron optics for low energy electrons (LEE, several volts up to several hundred volts) have been developed with a resolution in the nanometer range. One of the techniques referred to above, which nowadays is designated as Scanning Field-Emission Microscopy (SFEM), is essentially a Scanning Tunneling Microscope (STM) operated in the field-emission regime. The tip is retracted from the sample surface to distances greater than those typically employed in the STM (ranging from a few nanometers to a few tens of nanometers). By applying a negative bias to the tip, field

emitted electrons are focused and accelerated toward the sample by the strong field between the tip and the surface. Subsequent interaction with the solid leads to emission of a spectrum of electrons, which are detected at macroscopic distances.³ By scanning the tip, images of the topographic contrast as well as the magnetic signal of a sample have been obtained.⁴ The contrast mechanism of SFEM, which is essentially a development of the topographiner,⁵ is far from understood. In particular, how slow electrons emitted from near the point of impact of the primaries can travel through the strong tip-sample field remains unanswered. In fact, preliminary calculations⁶ of electron trajectories in vacuum show that the field in the tip-sample junction pushes all electrons generated at the impact position under the tip back into the solid, thus preventing them to reach the detector.

An essential improvement is obtained when electron trajectories in vacuum are described in a deterministic way,⁷ while the transport inside the solid is modeled in a stochastic manner.⁸ The latter part comprises multiple elastic and inelastic scattering as well as the generation of the cascade of secondary electrons and their escape over the

surface barrier. In this way, one can account for repeated re-entry and re-emission of electrons, i.e., events in which electrons “bounce” off the surface. In the present work, such a model has been studied. The results show a salient difference of the signal generation mechanism with respect to conventional secondary electron microscopy: the formation of a two-dimensional electron cascade, which propagates along the surface in the field between the electron source, the sample, and the (biased) detector. While elastically and inelastically backreflected electrons reaching the detector originate from locations close to the impact position, the detected secondary electrons are created far away, up to several hundred micrometers(!).

Simulations were carried out for a silver target and for a tip-sample configuration as shown in Fig. 1. Panel (a) shows the geometry of the SFEM, which is assumed to have cylindrical symmetry around the tip and the z -axis. Note that the calculation of the trajectories is a veritable three dimensional calculation, albeit in a cylindrically symmetric field. This tip geometry, shown in panels (b) and (c) of Fig. 1, consists of a cusp terminated by a spherical apex (with a radius of curvature of 5 nm) and is known to produce a realistic electric field.⁹ For the case depicted in Fig. 1, the target occupies the space $z \geq 0$ and is set at ground potential. The tip is set at a negative potential, and the distance between its apex and the target is taken to be 20 nm. Note that the tip bias voltage is equal to the landing energy of the electrons at the surface, E_0 , and that the assumed position of the primary impact is at zero depth. The lateral position of the tip coincides with the origin of the coordinate system. The parameters used in the simulation are chosen in accordance with experiment.³ In the half-space above the surface, the tip is surrounded by an annular detector [see panel (a) in Fig. 1], which is set to a positive potential (3 kV). The current model

does not account for the details of the field emission process at the tip and assumes the latter to behave as a pointlike source emitting electrons only from the very center of the tip apex. Under these conditions, the distribution of the points of impact of the primary electrons on the surface has a width well below a nanometer for electrons starting with thermal velocities in arbitrary directions at the location of the tip apex. This follows from simulations (not shown) for any reasonable combination of the tip-bias and tip-sample distance and demonstrates the strong focusing effect of the field in the tip-sample junction.¹⁰ To obtain a realistic focal width, the present results should be convoluted with the true spatial emission distribution at the apex, as dictated by the physics of field emission in the specific geometry considered.

In Fig. 2, representative results of 500 electron trajectories are shown for 200 eV electrons. They are emitted from a field-emission tip located 20 nm above the origin of the coordinate system, which is in the center of each panel. For clarity, only 50 trajectories are shown in panel (a). The panels in the left column represent the side view, while the top view is shown in the right column at the same scale, as indicated by the yellow scale bars. The color scale indicates the generation of the electrons in the cascade, i.e., a primary electron (dark blue) creates a first generation secondary by transferring energy and momentum to a solid state electron in an inelastic collision (light blue), which in turn creates a second generation secondary in a subsequent inelastic process (green), and so on. The orange annulus in panel (e) represents the detector in the considered configuration. It is seen in panel (a) that, inside the solid, the dissipation of the energy of 200-eV primary electrons gives rise to formation of a secondary electron cascade consisting of about seven generations, occupying a volume inside the solid approximately given by a half-sphere with a radius of ≈ 25 nm.

The energy loss of a fast electron in a solid is of the order of the energy of the solid state electrons (1 Hartree = 27.2 eV).¹¹ This is therefore the typical energy the first generation secondaries receive upon creation. For higher generation secondaries, the initial energy is slightly less than for the previous generation, and so on. Therefore, mainly backreflected primary electrons (dark blue) or first (light blue) and second (green) generation secondaries can escape over the surface potential barrier and make it into vacuum. In vacuum, the strong field between the tip and the sample pushes a large fraction of the cascade-electrons leaving the surface, especially those of higher generation, back into the solid. Notice, however, that due to the component of the field parallel to the surface, which is present everywhere except at the very lateral position of the tip (see Fig. 1), the re-entry position is displaced from the position of first impact by a significant distance. The effect of the field pushing back the electrons is most clearly distinguishable in the side-view panels (a)–(d), as well as the re-entry points scattered around the first impact position in the top view. Upon re-entry, the cascade is continued, but radially displaced, i.e., re-entering electrons can be elastically or inelastically scattered with the concomitant creation of the next generation of secondaries.

The lateral and depth scale on which the processes above and inside the solid take place can be inferred from Fig. 2, which shows that the maximum depth of the cascade amounts to about 25 nm. Owing to the comparatively huge distances the particles travel in vacuum, the lateral extent of the cascade achieves macroscopic dimensions up to several hundred micrometers. In this sense, one might indeed speak of a two-dimensional cascade leading to the signal formation in the SFEM.

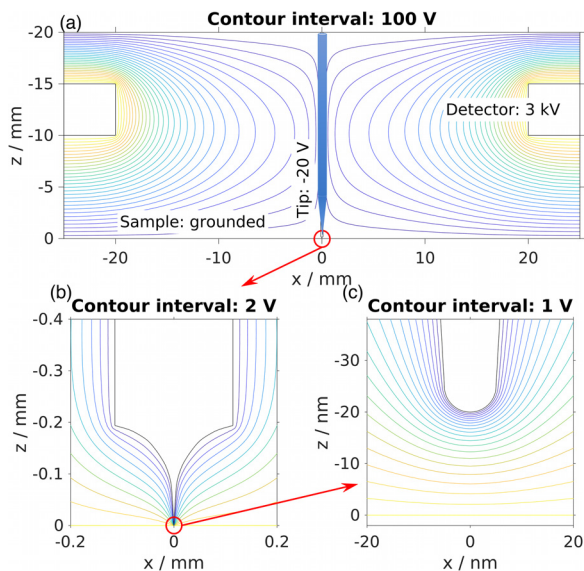


FIG. 1. Model geometry and equipotential lines of the calculated electrical field among the tip, sample, and detector. In the calculation of the field, a cylindrical symmetry has been assumed. Therefore, the detector, which is biased at +3 keV, is an annular structure. Note the dramatic difference in the dimensions of the 3 displayed panels: from centimeters in the upper panel to nanometers in the lower right panel. Describing the motion in vacuum therefore requires solution of a multiscale problem.

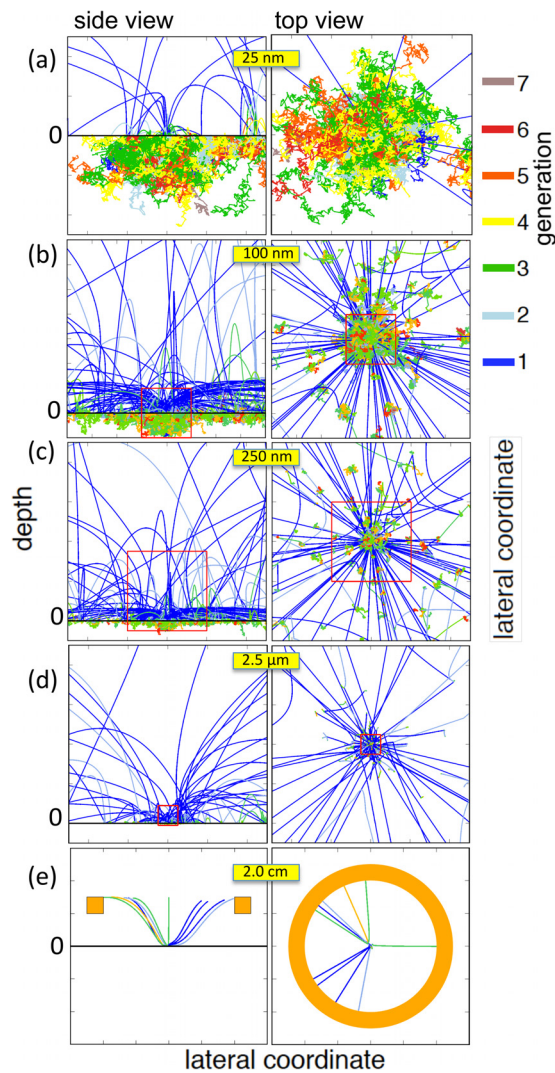


FIG. 2. Trajectories of 200 eV–primary electrons in and above a Silver target for a tip (not shown) located 20 nm above the surface at lateral coordinates (0,0). For this material, the work function used amounts to 4.3 eV, while the inner potential was 17.1 eV. Left column: side view, with the label “0” indicating the interface between the solid (below the horizontal black line) and vacuum (above). Right column: topview. From top to bottom (a)–(e), the field of view is zoomed out as indicated by the yellow size bars. The color scale indicates the generation of the secondaries (see the text).

Depending on the energy, there is a certain minimum distance from the emission location from which an electron needs to be emitted in order to reach the detector without being pushed back into the solid. Elastically backreflected electrons can always penetrate the field between the sample and the tip, since the tip-sample potential barrier provides the primary electron with a kinetic energy matching the tip-sample field. For secondary electrons with energies of the order of an electron volt, this distance amounts to a few tens of a micrometer up to a millimeter, as concluded from a series of simulations investigating this question (not shown).

The above explains why the seven electrons that reach the detector (out of 500) in the example shown in Fig. 2(e) are mainly backreflected primaries (blue). The secondary electrons of any generation that reach the detector are almost exclusively created at radial locations far away from the primary point of origin. This is most impressively demonstrated by the spectrum of electrons reaching the detector, shown as the multicolored upper spectrum in Fig. 3. Here, the radial distance from the tip at which the detected electrons originate is indicated by the color scale (given in millimeters). Those low energy secondaries reaching the detector are indeed created far away from the origin, while only the backreflected primaries originate from locations near the position of primary impact.

The partial spectra corresponding to a given number of re-entries (homogeneously colored curves) are shown in Fig. 3. While the elastic peak is made up of backreflected primary electrons that penetrate the surface exactly at the lateral location of the tip and reach the detector after bouncing off the surface one or more times, the peak below ~ 50 eV mainly consists of secondary electrons created far away from the tip (of the order of a millimeter). These secondaries are created by primaries that re-enter the solid several times. Most surprisingly, the peak below 50 eV (red curve) consists of secondary electrons created far away from the tip (see the upper curve of Fig. 3) that reach the detector only traveling in vacuum after they are emitted from the surface (far away from the origin), they do not re-enter the surface at all.

These observations draw a clear picture of the cascade, which consists of two main contributions: (1) elastically or inelastically backscattered primaries that penetrate the surface exactly at the lateral location of the tip and reach the detector after a given number of bounces; and (2) secondary electrons created as these primaries re-enter the solid at macroscopic radial distances from the primary impact position. For the former part of the cascade, the partial spectra shown in Fig. 3 give an impression of the typical number of re-entries.

The question remaining to be addressed is whether the proposed signal generation mechanism is in agreement with experiment. The experimental observations made so far show that (1) the yield (number of detected electrons per incoming electron) is very low—orders of magnitude below unity—making it cumbersome to

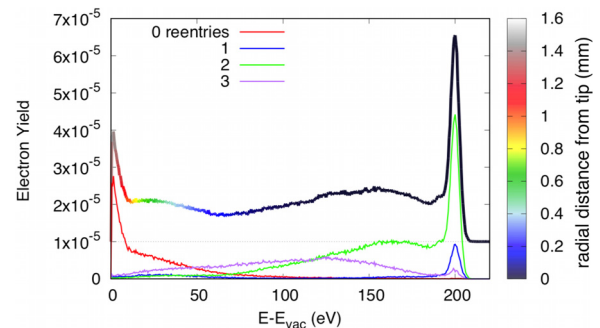


FIG. 3. Thick multicolored curve: energy spectrum of detected electrons with the color scale [in millimeters (!)] indicating the radial distance between the point of origin of the signal electrons from their point of origin. For backscattered electrons, the position of primary impact is taken to be the point of origin and for secondary electrons the location where they are generated. Partial spectra shown as homogeneously colored curves represent electrons reaching the detector after a given number of re-entries into the solid, as indicated in the legend.

experimentally distinguish between the tip current and the absorbed current;¹² (2) the achievable lateral resolution is of the order of a nanometer;^{6,12} (3) significant contrast is observed at surface locations consisting of different elements; (4) magnetic signal has been observed on magnetized samples using a Mott-detector.^{4,13}

To understand the observed contrast as described above, it should be recalled that a change in the work function of the solid sensitively influences the secondary electron yield, leading to contrast governed by the chemical state of the surface. On the other hand, the intensity of elastic scattering of the incoming electrons by the screened Coulomb field of the nuclei inside the solid is mainly governed by the atomic number of the scattering centers. This leads to intensities in the (in)elastically backscattered electrons depending on the element hit by the primary electrons and thus gives rise to elemental contrast.¹⁴ Work function changes only have a very minor influence on the backscattered electrons since the acceleration experienced due to the potential barrier upon entry of the solid is balanced by the deceleration upon exit. The present model calculations suggest that the contrast in the SFEM is produced by backreflected electrons implying elemental contrast. The model indeed predicts electron yields far below the typical yield for field-free detection (which is of the order of unity), while the effect of the field leads to a reduction of several orders of magnitude. This can be seen in the intensity scale in Fig. 3.

Magnetic contrast⁴ using an unpolarized probing beam on a magnetized sample can be produced either by slow secondary electrons whose spin is aligned by the magnetic field as it travels through the solid or by (in)elastically backreflected primary electrons.^{15–18} It is presently not clear which of the mechanisms above is responsible for the magnetic contrast, which has been observed in the SFEM with polarization analysis (SFEMPA).¹³

The question how a 2D-cascade of macroscopic dimensions gives rise to images with elemental, chemical, or magnetic contrast and a lateral resolution in the nanometer range seems to be more challenging. As discussed further above, the focusing effect of the field leads to a lateral distribution of primary impact not contradicting the experimentally observed lateral resolution. Let us assume for a moment that the number of backreflected electrons indeed depends on the atomic number of the scattering centers at the point of impact and that their energy suffices to make it to the detector after a given number of bounces. During imaging the tip is displaced over the surface by a fraction of a nanometer, while the cascade has macroscopic dimensions. The essential point is that the response of the cascade to the signal produced at the position of the tip at a given moment will always be the same since the tip displacement is negligibly small compared to the lateral extent of the cascade. If more (signal) electrons are produced at the tip location, more electrons will be created in the cascade and recorded by the detector. The sample surface acts as an electron multiplier, and since the location of origin of the signal electrons is always the same (within a few nanometers) compared to the huge extent of the cascade, the local contrast as sensed by the tip (with nanometer resolution) will be recorded by the detector.

In order to reconcile the concept of the 2D-cascade with the observation of magnetic contrast,⁴ it is useful to separately consider the two parts of the cascade, i.e., the backreflected primaries that reach the detector after a given number of bounces and the secondaries that are created far away from the impact position of the primaries and reach the detector without re-entry. For the backreflected part, assume

that the probability that the primary is spin-polarized as it is reflected from the target is given by P . Assume furthermore that during a bouncing process, the probability to forget the spin orientation received at the primary impact position is Q . Then, the fraction of electrons polarized according to the spin texture under the tip and reaching the detector will be $P(1 - Q)^n$, where n is the average number of bounces, $n \sim 2$ for the case studied in the present work (see Fig. 3). For any reasonable choice $0.1 < P, Q < 0.9$ of the individual probabilities, this results in a spin polarization of the detected signal of at least a few percent or more. The second part of the cascade, the secondary electrons created at macroscopic distances from the tip location, will not carry any signature of the magnetic structure probed by the tip as it scans across the surface and hence reduce the magnetic contrast.

The present model calculations, which combine deterministic propagation in vacuum and stochastic interaction of the signal electrons inside the solid, yield the concept of a 2D electron cascade, which may turn out to be very useful in describing the signal generation in the SFEM and related techniques. In this way, the very fact that electrons are indeed detected at all in an SFEM experiment in spite of the strong field pushing the signal electrons back into the surface is explained. The features of the cascade brought to light by the model do not contradict any of the experimental observations made so far. On the other hand, it makes clear predictions, such as the fact that the signal is effectively made up of backreflected electrons rather than slow secondaries created at the tip location, while those secondary electrons that reach the detector are created far away from the impact location.

Financial support by the FP7 People: Marie-Curie Actions Initial Training Network (ITN) SIMDALEE2 (Grant No. PITN 606988) is gratefully acknowledged. The computational results have been achieved using the Vienna Scientific Cluster (VSC).

REFERENCES

- ¹J. Goldstein, D. E. Newbury, P. Echlin, D. C. Joy, A. D. Romig, C. E. Lyman, C. Fiori, and E. Lifshin, *Scanning Electron Microscopy and X-ray Microanalysis* (Plenum, New York, London, 1992).
- ²O. L. Krivanek, T. C. Lovejoy, and N. Dellby, “Aberration-corrected STEM for atomic-resolution imaging and analysis,” *J. Microsc.* **259**, 165–172 (2015).
- ³D. A. Zanin, L. G. De Pietro, Q. Peter, A. Kostanyan, H. Cabrera, A. Vindigni, T. Bäler, D. Pescia, and U. Ramsperger, “Thirty percent contrast in secondary-electron imaging by scanning field-emission microscopy,” *Proc. R. Soc. A* **472**, 20160475 (2016).
- ⁴L. De Pietro, G. Bertolini, Q. Peter, H. Cabrera, A. Vindigni, O. Gürlü, D. Pescia, and U. Ramsperger, “Spin-polarised electrons in a one-magnet-only Mott spin junction,” *Sci. Rep.* **7**(1), 13237 (2017).
- ⁵R. Young, J. Ward, and F. Scire, “Observation of metal-vacuum-metal tunneling, field emission, and the transition region,” *Phys. Rev. Lett.* **27**, 922–924 (1971).
- ⁶H. Cabrera, “Analytical and numerical models for scanning field-emission microscopy and their experimental validation,” Ph.D. thesis, *ETH Zürich*, 2017.
- ⁷T. Radlička, M. Unčovský, and M. Oral, “In lens BSE detector with energy filtering,” *Ultramicroscopy* **189**, 102–108 (2018).
- ⁸O. Y. Ridzel, V. Astašauskas, and W. S. M. Werner, “Low energy (1–100 eV) electron inelastic mean free path (IMFP) values determined from analysis of secondary electron yields (SEY) in the incident energy range of 0.1–10 keV,” *J. Electron Spectrosc. Relat. Phenom.* (published online).

- ⁹A. Chatziafratis and J. Xanthakis, "Field emission from a nanometric paraboloidal emitter," *J. Electron Spectrosc. Relat. Phenom.* (published online).
- ¹⁰W. B. Su, C. L. Lin, W. Y. Chan, S. M. Lu, and C. S. Chang, "Field enhancement factors and self-focus functions manifesting in field emission resonances in scanning tunneling microscopy," *Nanotechnology* **27**, 175705 (2016).
- ¹¹W. S. M. Werner, "Electron transport in solids for quantitative surface analysis," *Surf. Interface Anal.* **31**, 141 (2001).
- ¹²D. A. Zanin, "Fundamental aspects of scanning field-emission microscopy and some similarities with critical phenomena," Ph.D. thesis (ETH Zürich, 2017).
- ¹³G. Bertolini, L. De Pietro, T. Bähler, H. Cabrera, O. Gürlü, D. Pescia, and U. Ramsperger, "Scanning field emission microscopy with polarization analysis (SFEMPA)," *J. Electron Spectrosc. Relat. Phenom.* (published online).
- ¹⁴F. Salvat, A. Jablonski, and C. J. Powell, "ELSEPA-Dirac partial-wave calculation of elastic scattering of electrons and positrons by atoms, positive ions and molecules," *Comp. Phys. Commun.* **165**, 157–190 (2005).
- ¹⁵S. N. Samarin, O. M. Artamonov, A. P. Baraban, M. Kostylev, P. Guagliardo, J. Berakdar, and J. F. Williams, "Elastic versus inelastic spin-polarized electron scattering from a ferromagnetic surface," *Phys. Rev. B* **94**, 155440 (2016).
- ¹⁶S. N. Samarin, J. F. Williams, A. D. Sergeant, O. M. Artamonov, H. Gollisch, and R. Feder, "Spin-dependent reflection of very-low-energy electrons from W(110)," *Phys. Rev. B* **76**, 125402 (2007).
- ¹⁷R. Feder, "Spin polarization in low-energy electron diffraction from nickel," *Phys Rev B* **15**, 1751 (1977).
- ¹⁸R. Feder, N. Müller, and D. Wolf, "Spin polarization in low-energy electron diffraction from Au(110): Theory and experiment," *Z. Phys. B* **28**, 265–271 (1977).